Unclassified

RT DOCUMENTATION PAGE

1a. [illegible]

1b. RESTRICTIVE MARKINGS

2a. [illegible]

3. DISTRIBUTION/AVAILABILITY OF REPORT
Approved for public release;
distribution unlimited

2b. DECLASSIFICATION/DOWNGRADING SCHEDULE

4. PERFORMING ORGANIZATION REPORT NUMBER(S)

5. MONITORING ORGANIZATION REPORT NUMBER(S)
AFOSR-TR- 89-0077

6a. NAME OF PERFORMING ORGANIZATION
University of Colorado at Boulder

6b. OFFICE SYMBOL (If applicable)
CEAE Dept.

7a. NAME OF MONITORING ORGANIZATION
AFOSR/NA

6c. ADDRESS (City, State and ZIP Code)
Boulder, Colorado 80309-0428

7b. ADDRESS (City, State and ZIP Code)
Building 410
Bolling Air Force Base
Washington, D.C. 20332-6448

8a. NAME OF FUNDING/SPONSORING ORGANIZATION
ZS-AF
Office of Scientific Research

8b. OFFICE SYMBOL (If applicable)
AFOSR/NA

9. PROCUREMENT INSTRUMENT IDENTIFICATION NUMBER
AFOSR-87-0363

8c. ADDRESS (City, State and ZIP Code)
Bld 410
Bolling Air Force Base
Washington, D.C. 20332-6448

10. SOURCE OF FUNDING NOS.

PROGRAM ELEMENT NO.	PROJECT NO.	TASK NO.	WORK UNIT NO.
61102 F	2302	C 2	

11. TITLE (Include Security Classification)
Brittle-Ductile Failure Mechanics of Concrete and Mortar

12. PERSONAL AUTHOR(S)
K.J. Willam, S. Sture, and V. Saouma

13a. TYPE OF REPORT	13b. TIME COVERED	14. DATE OF REPORT (Yr., Mo., Day)	15. PAGE COUNT
Final	FROM 8/15/87 TO 8/14/88	1988, October 14	20

16. SUPPLEMENTARY NOTATION

17. COSATI CODES		
FIELD	GROUP	SUB. GR.

18. SUBJECT TERMS (Continue on reverse if necessary and identify by block number)
Failure Mechanics of Concrete in Tension, Compression, Micromechanics, ~~of Particle~~ Matrix Composite

19. ABSTRACT (Continue on reverse if necessary and identify by block number)

The final technical report summarizes the results of the research effort related to the behavior of concrete on the:

- Experimental Level: Dilatancy and transition between brittle-ductile failure behavior in triaxial compression.
- Micromechanical Level: Numerical failure simulation of composite specimens in tension and compression. Voronoi polygonization of two phase mortar-aggregate composite. Probing of simple constitutive hypotheses for the constituents.

The numerical simulations depict the transition from distributed to localized failure when particle composites are subjected to tension and compression. The computational results show that tensile failure is definitely a surface-dominated process following fracture mechanics concepts in contrast to compressive failure.

20. DISTRIBUTION/AVAILABILITY OF ABSTRACT
UNCLASSIFIED/UNLIMITED ☒ SAME AS RPT. ☐ DTIC USERS ☐

21. ABSTRACT SECURITY CLASSIFICATION
Unclassified

22a. NAME OF RESPONSIBLE INDIVIDUAL	22b. TELEPHONE NUMBER (Include Area Code)	22c. OFFICE SYMBOL
Dr. Spencer T. Wu	(202) 767-6962	AFOSR/NA

DD FORM 1473, 83 APR EDITION OF 1 JAN 73 IS OBSOLETE.

Unclassified
SECURITY CLASSIFICATION OF THIS PAGE

AFOSR-TR- 89-0077

Brittle-Ductile Failure Mechanics of Concrete and Mortar

Kaspar Willam, Thomas Stankowski, Stein Sture and Victor Saouma
University of Colorado at Boulder

October 14, 1988

Abstract

Incremental collapse analysis invariably involves simulation of failure mechanisms of *"distributed"* or highly *"localized"* nature.

The report describes current work on the progressive failure behavior of concrete. After a brief review of experimental failure observations in tension and compression the issues of *"normality"* and *"characteristic length"* are discussed when describing localized changes of the internal structure during progressive failure. To this end the internal microstructure of concrete is considered to form a two-phase particulate composite made of elastic aggregate embedded in inelastic mortar. The paper examines the degradation of macroscopic stiffness and strength with the aid of numerical simulation of the mortar-aggregate composite. The computational results provide new insight into the distributed and localized nature of tensile and compressive failure processes for comparison with experimental observations on concrete composites.

1 Introduction

In view of the importance of reliable safety assessments there is an increasing demand for accurate failure predictions which trace the response behavior beyond the framework of well-posed initial boundary value problems. Progressive de-stabilization of the spatial and temporal discretization invariably leads to loss of single-valued solution regimes. It remains to construct computational strategies which not only survive but also reproduce the actual failure progression.

The computational difficulties are compounded by the fact that peak and post-peak response phenomena are really the manifestations of dramatic changes of the microstructure which can no longer be considered material properties. One of the main difficulties is therefore the extraction of fundamental fracture properties from servo-controlled laboratory experiments on specimens which are tested beyond peak into the post-peak regime. Backward identification of the governing fracture parameters, such as the characteristic width of the localized failure band and the dilatancy during progressive failure, involves the analysis of discontinuities and is one of the

pressing issues of failure mechanics, see recent review by Bazant [1].

In the case of concrete and other cementitious composites very different failure modes can be mobilized. They depend primarily on the type of loading and range from very localized mechanisms in tension to very distributed failure in confined compression. The success of computational failure simulations depends critically on the macroscopic constitutive model. Aside from proper initiation conditions realistic failure formulations have to capture fracture propagation and thus the drastic transition from very brittle to very ductile fracture as a fuction of confinement, see Hegemier and Read [2] as well as Horii and Nemat-Nasser [3].

In the first part, the paper summarizes experimental observations of triaxial failure in tension and compression. In the second part, current constitutive developments are briefly discussed with respect to their ability to predict failure. In the third and last part, the question is examined, whether the heterogeneous nature of concrete does affect initiation as well as propagation of failure in tension and compression. Thereby it is understood, that the size of the largest aggregate introduces an internal material scale which controls the distribution of initial microdefects and thus the location of initial failure mechanisms. The question arises, to what extent does the internal micro-structure influence the critical fracture path in tension and compression during coalescence of microdefects into the critical macrodefect? In broader terms, we ask whether the macroscopic failure mode depends on the internal micro-stucture and the *"critical failure path"* in the particulate composite and whether the macroscopic degradation of strength and the dilatancy are affected altogether?

1.1 Experimental Observations of Concrete Failure

The failure behavior of concrete is governed by complex degradation processes within the matrix-aggregate composite.

In direct tension, we observe a very brittle separation process which results in the formation of highly localized tensile cracks. The direct tension experiments by Reinhardt [4], Gopalaratnam and Shah [5] and Hurlbut [6] on cylindrical specimens of different height showed that the formation of macroscopic discontinuities is attributed to a surface-dominated failure process in the spirit of fracture mechanics. In fact, the results of the direct tension experiments depicted in *Fig.*1 illustrate the brittle nature of concrete with a well defined and stable post-peak regime. They exhibit a surprising amount of residual tensile strength due to 'teething' with relatively little stiffness degradation before and after peak. In sum, tensile cracking is a fracture phenomenon in spite of the tortuous character of the crack surfaces in the matrix-aggregate composite.

At low confined compression, we observe a more gradual degradation process of strength which is accompanied by highly dilatant behavior in the lateral direction. The uniaxial compression experiments by von Mier [7] on prismatic specimens of different height suggest that compressive failure is also dominated by fracture processes

which are however more distributed as we increase the level of lateral confinement. *Fig.*2 illustrates the large differences in the load-deformation behavior of cylindrical specimens subject to different levels of lateral confinement. The experimental results, which are extracted from the comprehensive test series by Smith [9], exhibit the rapid increase of strength and ductility with virtually intact elastic unloading behavior. In fact, there is a transition point TP of brittle-ductile fracture which separates softening of the macroscopic strength from highly ductile failure regimes in which virtually no degradation of strength is observed.

The schematic plot in *Fig.*3 delineates the different failure modes in the Rendulic stress plane. The narrow softening zone extends from tension into the low confined compression regime up to the transition point of brittle-ductile fracture. The failure regions beyond the transition point are very ductile and engulf a wide region of hardening behavior in triaxial compression which are compactive near the hydrostat and which turn gradually dilatant in the vicinity of the failure envelope. These observations are based on pertinent triaxial load history experiments which have been computerized by Stankowski [8] in the *"triaxial data base manual"* for concrete comprising stress-strain histories of 136 experiments. The global failure mechanisms below the transition point differ strongly when the response in triaxial compression is compared with that in triaxial extension. In fact, cylindrical fracture in the form of *"orthogonal"* cleavage is responsible for rather ductile softening on the macroscopic level. This failure in triaxial compression is primarily due to the excessive lateral tensile strains in the radial and circumferential directions when confined cylindrical test specimens are subjected to increasing axial compression. On the other hand, *"planar"* separation is responsible for very brittle softening on the macroscopic level due to excessive axial tensile strains when cylindrical specimens are subject to increasing lateral confinement in triaxial extension.

This overview of triaxial deformation and failure mechanisms sets the stage for physically motivated concrete model which should reproduce the following features in the pre- and post-peak regimes:

- There exists a transition point of brittle-ductile fracture which separates softening from hardening behavior,
- The degradation of strength in tension as well as in compression is caused by fracture processes of the internal composite structure resulting in macroscopic softening,
- There are two distinct modes of cylindrical and planar failure which are associated with orthogonal and planar cleavage in triaxial compression and triaxial extension,
- The lateral deformation behavior is characterized by loss of normality. Thus non-associated flow determines the amount of inelastic dilatancy and also the triaxial strength when strain control prevails.

In sum, the pressure-sensitive failure envelope differs markedly between loading paths in triaxial compression and triaxial extension. Moreover, hardening as well as softening response functions depend strongly on the lateral confinement. Thus the traditional plasticity concept of a 'universal' equivalent stress-strain relation has to be extended in order to account for the large increase of ductility with increasing confinement. Finally, the nonlinear compactive behavior in the vicinity of the hydrostat supports the notion of a cap. The inelastic dilatancy in the dilative cone and the compactive cap regions however requires direct control in the form of non-associated flow separately from the yield condition.

1.2 Normality of Inelastic Dilatancy

The non-associated formulation determines primarily the amount of inelastic dilatancy and thus the lateral deformation behavior in stress-controlled environments. On the other hand, in strain-controlled environments it is important to realize that normality severely overpredicts the triaxial strength because of the excessive dilatation which is converted into excessive lateral confinement. Therefore, inelastic dilatancy control is not merely benefiting the lateral deformation characteristics, it determines the strength and thus the ductility of the response predictions in strain-controlled environments.

*Fig.*4 taken from the recent experiments by S. Smith [9] illustrates the directions of the inelastic strain rates which are superimposed on the corresponding stress path of the triaxial compression tests at different confinement. Assuming negligible degradation of the elastic properties the total deformation measurements can be decomposed into the sum of elastic and inelastic components. The angle of the inelastic strain rate component with the hydrostat provides a measure of dilatancy which is invariably smaller than the corresponding friction angle, i.e. the normal to the current loading surface. This experimental observations agrees with the general opinion that frictional materials are non-associative and involve therefore non-symmetric constitutive operators. Another feature of this loss of normality is depicted in *Figs.*5 and 6 where the results of the *"wedge test"* are shown. This experiment was carried out in response to the recent discussion by Sandler and Rubin [11] who demonstrated analytically that loading into the wedge region is synonymous to negative energy dissipation and thus leads to instability. *Fig.*6 verifies this argument with respect to the loss of positive plastic work increment, i.e $d^2W_p = \int \dot{\sigma}\dot{\epsilon}dv < 0$. However, this is only a sufficient condition and not a necessary one. In fact, the specimen remained fully intact under load control inspite of the negative incremental plastic work.

In view of the prevalent displacement setting of the majority of finite element programs normality or rather the loss of normality, is an extremely important feature which can alter totally the triaxial response predictions. The dramatic effect of associated versus non-associated flow is illustrated with a model problem taken from the recent thesis by Pramono [12]. In that case the Leon failure model [13] is subjected to a strain path extracted from a triaxial compression experiment at $\sigma_r = 200\ psi$ confinement. Assuming in both cases perfectly plastic behavior the response predictions of associated versus non-associated flow are totally different, when the plastic poten-

tial of the non -associated formulation is governed by the pressure insensitive Tresca criterion. The response predictions are shown in *Fig.7* for the two models. After the failure envelope has been reached, the stress path of the associated flow rule moves up the failure envelope until a point is reached, where the prescribed strain increment is equal and coaxial with the plastic strain increment. On the stress-strain level this results in an excessive axial strengt'. prediction with unrealistically ductile behavior in the form of perfectly plastic flow. Conversely, the non-associated flow rule moves the stress path down the failure envelope into the tension region. On the stress-strain level this results in a reasonable prediction of axial strength with post-peak behavior which is too brittle and exhibits too rapid degradation of the residual strength.

These totally opposite response predictions demonstrate the fundamental role of the dilatancy on the overall strength and ductility behavior of pressure sensitive models.

2 Current Constitutive Issues

Current concrete models are either based on nonlinear elasticity, or on alternative plasticity, continuous damage and fracture mechanics theories respectively. The large number of recent publications are thus of little surprise, ([14], [15], [16], [17], [18], [19], [20], [21], [22], [23], [24], [25]) since none of these frameworks adequately descibes the entire spectrum of deformation and failure behavior of concrete. In view of the severe shortcommings of most formulations, it is imparative to verify these phenomenological constitutive models by micromechanical investigations, partly because of the limited number of experiments which are available for calibration and verification [8].

In the context of micromechanics it is instructive to recall some major results of composite mechanics, see ref. by Hashin [26]. In the case of *"isotropic composites"* made of a matrix and much stiffer and stronger spherical particles the effective composite properties depend primarily on the volume fractions of the constituents. While the elastic stiffness properties can be increased up to four or five times the matrix stiffness, the strength of such composites is only of the order of the matrix strength and may be even lower. The stiffness and strength of the composite increases when elongated particles are used, however, at the price of lower attainable volume fractions. For particulate composites the fundamental postulate of heterogeneous media states: *"The stress and strain fields in a large heterogeneous body subjected to homogeneous boundary conditions are statistically homogeneous, except in a boundary layer near the external surface"*. The formulation of effective elastic properties of composite materials centers around the concepts of *"Representative Volume Elements"* and *"Statistical Homogeneity"*. The notion of an equivalent continuum involves three characteristic length scales,

- the micro -scale, which is of the size of characteristic particle diameters,
- the meso(mini)-scale, which corresponds to the size of homogeneized representative volume elements, and
- the macro-scale, which is of the dimension of the composite material body.

In the following we examine tensile and compressive failure mechanisms on the meso-level. The geometry of the two-phase composite body is in this case assumed to be of the same size as the representative volume element. For concrete this dimension is usually at least six times the maximum aggregate size for which statistical homogeneity may be adopted. The main intent is to gain new insight into the evolution of the underlying failure processes in particle composites for which quantitative results are extremely difficult to obtain from macroscopic experiments. The study provides also a testbed for probing different constitutive hypotheses such as Mode I controlled failure mechanisms and their effects on the macroscopic behavior.

3 Numerical Simulation of Particle Composite

The numerical simulation of the two-phase mortar-aggregate composite is approached on two levels: First, the geometry and topology of the phase interface geometry is generated in random manner in order to define the configuration of representative composite bodies. Second, the response behavior is evaluated deterministically when the composite samples are subjected to prescribed load histories probing elementary constitutive assumptions for the physical properties of the two constituents.

3.1 Geometry and Topology of Mortar-Aggregate Phases

Concrete is a multiphase material comprised of well-graded aggregate, hydrated cement paste and voids. Since not every particle or void can be considered explicitely, the numerical simulation is confined to a two-phase matrix-particle composite in which only the larger inclusions are accounted for. Opposite to the deterministic generation of *"Numerical Concrete"* based on morphological descriptions by Roelfstra and Wittmann [27] the mortar-aggregate composite is here described in terms of polygonal approximations of crushed angular aggregate particles which are embedded in the mortar matrix in a random manner. The polygonal description was adopted earlier by Cundall et al. [28] for the idealization of granular solids with rigid particles and sliding interfaces, also known under the name of the *"Distinct Element Method"*. In our case, the composite body is subdivided into *Voronoi-Polygons* [29] centered around poles which are randomly distributed trough *Monte Carlo* perturbation of a regular grid.

The interface geometry of the mortar-aggregate composite is generated as follows: A systematic decision tree identifies *"non-contiguous"* aggregate polygons by shrinking the size of the original polygons in a random, non-affine manner. *Fig.*8 illustrates the composite geometry generated by this non-contiguous approach allowing direct control of the aggregate area fraction. In the subsequent simulation an aggregate area fraction of 50% is used throughout.

The gradation of the composite is characterized by the cumulative size distribution of aggregate particles. The sieveline in *Fig.*9 illustrates the aggregate distribution generated by the non-contiguous inclusion strategy, whereby smoother distributions could have been attained by refining the grid and appropriate spacing. The resulting

size distribution is certainly satisfactory in view of the limitations inherent in the two-dimensional idealization of the three-dimensional microstructure.

The two-dimensional finite element discretization with 2352 DOF is shown in *Fig.*10 which also depicts the idealizations of the two constituents. Each polygon is subdivided into triangular element patches made of four or nine constant strain triangles which span between two adjacent vertices and the centroid of the polygon. The complex idealization illustrates the need for automatic pre- and post-processing with renumbering and band optimization. We also note the rapid growth of elements and number of degrees of freedom, DOF, when the polygonization is refined for better gradation. In fact, the more appropriate three-dimensional simulation of the composite is simply beyond current computational means, although conceptually, it does not require development of new features.

3.2 Material Description of Constituents

The main objective of this study is to evaluate the influence of the composite action on the failure mechanisms in concrete. Therefore, only elementary constitutive assumptions are adopted for each of the constituents in order to quantify the composite effect on the macroscopic manifestations of localized failure.

In the computational failure study the aggregate-phase is assumed to remain in the linear elastic response regime. This constitutive postulate is fairly realistic for low and medium strength concretes with stiffness and strength properties of the aggregate particles which are substantially greater than those of the mortar.

The scope of the current composite study is limited to an elastic-plastic *Drucker-Prager* formulation of the mortar matrix with decohesive softening in the post-peak regime. *"Normality"* is assumed in order to quantify the loss of associated flow on the macroscopic level. Thus, the friction angle is kept constant during plastic flow and coincides with a dilatancy angle of $\Phi = 30^o$ for the matrix constituent. Furthermore, no characteristic length is introduced to regularize the softening computations and to minimize mesh size dependence [30], [31]. In fact, the composite argument opens the question, whether the characteristic length is redundant altogether since distributed stress concentrators at aggregate vertices trigger crack initiation in a fairly distributed fashion?

We recall that associated flow results in highly dilatant behavior and in excessive confinement when plane strain conditions are adopted. In return, this passive confinement leads to gross overprediction of mortar strength when high dilatancy angles are used. Thus plane stress conditions are adopted for the inelastic response analysis in which the internal friction angle of $\Phi = 30^o$ assures closure of the failure envelope in biaxial compression. The analysis is carried out with the nonlinear finite element program Microfem [32] in which the invariant response formulation [33] has been implemented for the general description of frictional materials. *Fig.*11 summarizes the properties of the *Drucker-Prager* model and the softening properties in uniaxial ten-

sion. Although the low softening modulus results in far too ductile behavior in direct tension, it is required to assure stable post-peak control and to avoid snap-through phenomena particularly in biaxial compression.

The material behavior of the mortar-aggregate interface is depicted in *Fig.*12 for tensile failure which is mobilized when the current value of degrading bond strength is exceeded. This approach monitors constant values of the fracture energy release rate in terms of the crack opening displacement, whereby the shear stiffness diminishes to zero when the residual tensile strength has been exhausted. In sum, the present interface model allows to investigate two extreme cases, (i) full bond without degradation of the interface behavior, and (ii) purely tensile debonding without shear transfer beyond critical crack-opening.

4 Computational Results

The investigation of the matrix-aggregate composite is comprised of four parts: The first study is focussed on the elastic properties of the composite for various ratios of elastic phase moduli. The next two investigations examine the tensile and compressive failure mechanisms in rectangular composite bodies with different aspect ratios. The fourth study considers compressive and tensile load-histories during which a composite specimen is preloaded in one direction and subsequently unloaded and reloaded in the orthogonal direction up to failure. In most cases monolithic contact i.e. full bond is assumed between aggregate and mortar. In few cases tensile debonding is permitted in order to study the influence of degrading interface properties surrounding each aggregate particle during failure progression.

4.1 Effective Elastic Properties of Particle Composite

In the first study we examine the effect of different elastic mortar and aggregate properties. This topic is normally pursued within the framework of composite mechanics with mixture rules which define the effective stiffness properties of the overall composite. The results of the two-phase particle composite are shown in *Fig.*13 for the random distribution of polygonal inclusions. The four diagrams depict the change of composite stiffness when the ratio between aggregate/matrix moduli varies between one and ten for the aggregate concentration of 50%.

Clearly, the random arrangement of inclusions leads to composite stiffness properties which lie between the two limiting cases of the series and parallel arrangement of the two constituents. The results of the numerical simulation agree surprisingly well with the analytic estimates by Hashin [34] for non-contiguous spherical inclusions and low level particle concentration. Altogether the graphs of *Fig.*13 indicate that the series model provides a lower bound of the overall stiffness which exceeds the mortar stiffness merely by 70%. On the other hand, the parallel model leads to a linear increase of the composite stiffness which grows proportionally to the aggregate stiffness and the phase concentration.

The angular particle composite exhibits elastic stiffness properties which are asymptotically controlled by the elastic properties of the contiguous matrix surrounding each particle. In fact, the normalized values of the effective composite stiffness inreases in our case not more than three times the value of the matrix stiffness. The same observation holds for the composite strength in tension which is essentially controlled by that of the mortar matrix with $f_t' = 0.82\ Ksi$, see *Fig.*14. This figure also illustrates the isotropy of stiffness and strength, when the composite body is subjected to two separate tensile load histories in x- and y-directions. In contrast, *Fig.*15 depicts the results of two analogous experiments in uniaxial compression. Again, the stiffness of the composite body exhibits full isotropy as expected, however the uniaxial strength values differ considerably in x- and y-directions. Note that both composite strength values exceed the nominal strength $f_c' = 2.0\ Ksi$ of the mortar matrix, in spite of the homogeneous boundary conditions adopted for the numerical experiments. In contrast to the tensile strength of particle composites, the heterogeneous microstructure increases the compressive strength of the composite body beyond that of the mortar matrix, because of the locking block action of the aggregate particles embedded in the frictional mortar matrix.

Three specimen geometries are examined in order to address the issue of surface versus volume-dominated failure processes in direct tension and uniaxial compression. The results of the square specimen with the aspect ratio of $h/l = 1$ are denoted by the symbol $(4 * 4)$, while those of the rectangular specimens with the aspect ratios $h/l = 2$ and $h/l = 0.5$ are designated by the symbols $(8 * 4)$ and $(2 * 4)$. The stiffness ratio $E_a/E_m = 5$ is used throughout the investigation for the matrix-aggregate composite. The gradually increasing load is applied under mixed control with full lateral restraint at the top and bottom faces of the specimen simulating the effect of rigid loading platens. Thus, both the micro-structure as well as the lateral restraint influence the strength and the localization process at failure.

4.2 Tensile Failure Simulations

*Fig.*16 illustrates the overall response behavior of the square specimen subjected to direct tension. The results are plotted in terms of nominal values of stresses and strains which are extracted from the reactions and the relative displacements between the boundaries of the finite element idealization.The response predictions compare well with experimental results in direct tension, particularly when the localization at peak and the progressive separation in the post-peak regime are considered. The active zones of plastic dissipation are inserted in *Fig.*16 in order to visualize the progressive failure process in tension. The three plots exhibit different failure stages in the pre- and post-peak regimes. The distributed cracking mode in the pre-peak regime is followed by strong redistribution during the formation of a single transverse crack which separates the composite specimen from the loading platen near the bottom face.

The post-peak results of the three specimens with different heights are summarized in *Fig.*17. The tall specimen exhibits only slightly more brittle behavior during sep-

aration than the compact specimen. In fact, the three post-peak slopes do not differ enough to contradict the concepts of fracture mechanics for interpreting the separation process in tension. Recall, that the area under the nominal tensile stress versus crack opening displacement curve is a measure of the fracture energy release rates for the three different specimen heights. The agreement confirms previous experimental observations on tensile failure of different height specimens [35], where the fracture energy release rate remained fairly constant during formation of the transverse crack. In sum, tensile softening is a surface- rather than a volume-controlled fracture phenomenon.

The question of the characteristic length is addressed in *Fig.*18. The plot depicts the locations of interface elements in the square specimen which are subjected to tensile failure at an overall load level corresponding to 75% of the tensile peak load. Recall that the polygonal particles are surrounded by interface boundary layers with 50% higher debonding strength than the contiguous mortar. This premature debonding in the interface elements is mobilized in spite of their high debonding strength, because the interface stresses are dominated by the high stress level in the stiff aggregate particles. In spite of these stress concentrators the tensile cracking path is ultimately forced through the mortar matrix because of the non-contiguous distribution of aggregate particles and the disconnected network of interface boundaries. The plot clearly underlines the distributed nature at crack initiation which is governed by the location of aggregate particles. However, the final separation process develops in the form of a single discontinuity across the mortar matrix with contiguous zones of elastic unloading. Thus, we may conclude that the final separation process is a structural phenomenon which affects the entire specimen due to localization into active zones of high energy dissipation and large contiguous blocks of elastic unloading.

4.3 Compressive Failure Simulations

For tensile strength degradation it is widely accepted that tensile cracking is governed by fracture mode I. The question, whether fracture mechanics also governs the failure process in compression, is debated vigorously with respect to the issue, whether there exists a critical fracture energy release for mode II-type fracture for brittle solids independently of mode I. For this reason the numerical simulations of the tension experiments above are now repeated for the case of uniaxial compression.

The compressive response behavior is shown in *Fig.*19 for the square composite specimen. The inserts in the figure provide some insight into the failure patterns which develop in the pre- and post-peak regimes. The elementary *Drucker-Prager* model of the mortar matrix does result in shear-type failure modes which agree surprisingly well with the experimental observations reported by von Mier [7]. Although the multiple shearing planes are partially induced by the boundary conditions, the final conical failure mode emerges along weak shear planes in the contiguous mortar matrix. Opposite to the response behavior in direct tension the matrix-dominated shear failure leads to an increase of the uniaxial compressive strength of the composite beyond the mortar strength. The numerical simulation illustrates the frictional strengthening due

to composite action. In that case, both strength and softening behavior are clearly influenced by the microstructure of the mortar-aggregate composite.

The issue of surface- versus volume-dominated failure mechanisms in compression is addressed in *Fig.*20. The plots depict the post-peak response behavior of three composite specimens with different heights. The different softening slopes indicate that the fracture energy release rate varies strongly with specimen height, quite in contrast to the experimental observations reported by von Mier [7]. On the other hand it is intriguing that normalizing the axial displacements by the three specimen heights leads to strain-softening response diagrams which agree fairly closely. In other terms, the numerical experiments in compression support the notion of volume- rather than surface-dominated failure processes.

4.4 Compressive and Tensile Failure Simulations with Orthogonal Preloading

In the final study we examine the effect of preloading on the stiffness and strength of square composite specimens in which the direction of loading is rotated by 90° at different states of damage. To this end a number of virgin composite specimens were first loaded uniaxially in the y-direction up to a prescribed level of preloading and subsequently unloaded and reloaded in the x-direction.

The compressive results are shown in *Fig.*21 depicting the strong degradation of compressive strength because of preloading in the orthogonal direction. The analogous simulation in tension shown in *Fig.*22 exhibits far less strength degradation inspite of tensile preloading beyond peak. The same preloading effects in tension and compression were reported by von Mier [7] who discerned in his concrete experiments between 'cylindrical' and 'planar' modes of failure which are accompanied by totally different changes of the internal microstructure. In compression, the inclined mode of failure takes place simultaneously in two orthogonal directions. Therefore, reloading in the orthogonal direction is strongly influenced by the level of preloading.

*Fig.*23 illustrates the different stages of inclined failure during compressive preloading in the y-direction and subsequent compressive loading in the x-direction. In contrast, *Fig.*24 depicts the localized failure modes in tension which are virtually orthogonal to the two tensile load directions with little interaction.

In sum, the numerical load history experiments clearly exhibit the directionality of progressive failure and the related differences between tensile and compressive strength degradation of specimens preloaded previously in orthogonal direction.

5 Concluding Remarks

The composite simulation provides new insight into the failure mechanisms which take place in the heterogeneous matrix-aggregate composite. The computational results

indicate that the initial failure mechanisms are very distributed both in tension and compression. Only the final stage of the tensile separation process is truly localized. In that case fracture mechanics prevails in form of a surface-dominated process with a characteristic length which is of the same order of magnitude as the specimen geometry. This localization mode is accompanied by dramatic strain redistribution which requires dynamic enrichment or realignement of the finite element mesh and endowment of the constitutive operator by a characteristic length to delimit the zones of active failure. On the other hand, the failure mechanisms in compression exhibit fracture properties which differ substantially from those in tension.

References

[1] Bažant, Z.P.(1986). "Mechanics of Distributed Cracking," *Appl. Mech. Rev.*, Vol. 39, No. 5, pp. 675–705.

[2] Hegemier, G.A. and Read, H.E. (1985). "On deformation and Failure of Brittle Solids, Some Outstanding Issues," *Mechanics of Materials*, Vol. 4, pp. 215–259.

[3] Horii, H., and Nemat Nasser, S. (1986). "Brittle Failure in Compression: Splitting, Faulting and Brittle-Ductile Transition", *Phil. Trans. Royal Soc.*, London, Vol. 319, No. 1549, pp. 337–374.

[4] Reinhardt, H.W. (1984). "Fracture Mechanics of an Elastic Softening Materials Like Concrete," *Heron*, Vol. 29, No. 2, pp. 42.

[5] Gopalaratnam, V.S. and Shah, S.P. (1984). "Softening Response of Concrete in Direct Tension," Technological Institute Report, Dept. of Civil Engineering, Northwestern University, Evanston.

[6] Hurlbut, B.J. (1985). "Experimental and Computational Investigation of Strain-Softening in Concrete," M.S. Thesis, CEAE Department, University of Colorado, Boulder.

[7] von Mier, J.G.M. (1984). "Strain-Softening of Concrete under Multiaxial Loading Conditions", Ph-D. Dissertation, De Technische Hogeschool Eindhoven, Netherlands.

[8] Stankowski, T. (1987) "Database Manual of Triaxial Load History Experiments on Plain Concrete," *Structures Research Report*, University of Colorado Boulder.

[9] Smith, S.S. (1987). "On Fundamental Aspects of Concrete Behavior", M.S. Thesis, CEAE Department, University of Colorado, Boulder.

[10] Smith, S.S., Willam, K.J., Gerstle, K.H., Sture, S. (1988). "Concrete over the Top — or: Is there Life after Peak", *Journal of ACI*, accepted for publication.

[11] Sandler, I.S. and Rubin, D. (1987). "The Consequences of Non-Associated Plasticity in Dynamic Problems", *Proc. Intl. Conf. on Constitutive Laws for Eng. Matls.*, Tucson Arizona, Eds: C. Desai et al., Vol. 1, Elsevier, New York.

[12] Pramono, E. (1988). "Numerical Simulation of Distributed and Localized Failure in Concrete," Ph.-D. Dissertation, CEAE Department, University of Colorado, Boulder.

[13] Romano, M. (1969). "On Leon's Criterion", *Meccanica*, pp. 48–66.

[14] Chen, E.S. and Buyukozturk, O. (1985). "Constitutive Model for Concrete in Cyclic Compression," *Journal of Engineering Mechanics*, ASCE, Vol. 111, No. 6, pp. 797–814.

[15] Han, D.J. and Chen W.F. (1985). "A Nonuniform Hardening Plasticity Model for Concrete Materials," *Proc. Inelastic Deformation and Failure Modes*, S. Nemat-Nasser ed., pp. 238–308.

[16] Klisinski, M. (1985). "Degradation and Plastic Deformation of Concrete," IFTR Report No. 38, Polish Academy of Sciences, Warsaw, pp. 198.

[17] Levine, H.G. (1982). "A Two Surface Plastic and Microcracking Model for Plain Concrete," *ASME Symposium Volume 82 — 79178*, L. Schwer ed., New York, pp. 27–48.

[18] Ortiz, M. (1984). "A Constitutive Theory for the Inelastic Behavior of Concrete," *Mechanics of Materials*, Vol. 4, pp. 67–93.

[19] Schreyer, H.L. and Babcock, S.M. (1985). "A Third Invariant Plasticity Theory for Low-Strength Concrete," *Journal of Engineering Mechanics*, ASCE, Vol. 111, No. 4, pp. 545–558.

[20] Shafer, G.S. and Ottosen, N.S. (1985). "An Invariant-Based Constitutive Model," Structural Research Series No. 8506, CEAE, University of Colorado.

[21] Stankowski, T. and Gerstle, K.H. (1985). "Simple Formulation of Concrete Behavior under Multiaxial Load Histories," *Journal of ACI*, Vol. 82, pp. 213–221.

[22] Valanis, K.C. and Read, H.E. (1984). "An Endochronic Plasticity Theory for Concrete," S-Cube Topical Report, La Jolla, pp. 93.

[23] Willam, K., Ko, H.Y., Sture, S., Gerstle, K., Pramono, E., Stankowski, T., Klisinski, M., and Smith, S. (1987). "Constitutive Driver for Triaxial Response Behavior of Plain Concrete," Structural Research Series No. 87–08, University of Colorado, Boulder.

[24] Yang, B.L., Dafalias, Y.F., and Herrmann, L.R. (1985). "A Bounding Surface Plasticity Model for Concrete," *Journal of Engineering Mechanics*, ASCE, Vol. 111, No. 3, pp. 359–380.

[25] Pramono, E., and Willam, K. (1988). "Fracture Energy-Based Plasticity Formulation of Plain Concrete", *Journal of Engineering Mechanics*, accepted for publication.

[26] Hashin, Z. (1983). "Analysis of Composite Materials-A Survey", *J. Appl. Mech.*, Vol. 50, pp. 481–505.

[27] Roelfstra, P.E., Sadouki, H. and Wittmann, F.H. (1985). "Le Béton Numerique", *Materials and Structures*, Rilem, Vol. 18.

[28] Cundall, P.A. and Strack, O.D.L. (1979). "A Discrete Numerical Model for Granular Assemblies", *Geotechnique*, Vol. 29, pp. 47–65.

[29] Finney, J.L. (1979). "A Procedure for the Construction of Voronoi Polyhedra", *J. Comp. Physics*, Vol. 32, pp. 137–143.

[30] Bazant, Z.P., and Oh, B.K. (1983). "Crack Band Theory for Fracture of Concrete", *Materials and Structures*, Rilem, Vol. 16, pp. 155–177.

[31] Willam, K., and Montgomery, K. (1987). "Fracture Energy-Based Softening Plasticity Model for Shear Failure", *Proc. Intl. Symp. on Interact. of Non-Nuclear Munition with Struct.*, Vol. II, Mannheim, March 1987, pp. 679–691.

[32] Montgomery, K. (1988). "Finite Element Analysis of Concrete Structures", MS-Thesis in Civil Engineering, University of Colorado at Boulder.

[33] Shafer, G.S., and Ottosen, N.S. (1985). "An Invariant-Based Constitutive Model", Structural Research Series No 8506, University of Colorado, Boulder.

[34] Hashin, Z. (1962). "The Elastic Moduli of Heterogeneous Materials", *J. Appl. Mech.*, Vol. 29, pp. 145–154.

[35] Willam, K., Hurlbut, B., and Sture, S. (1986). " Experimental and Constitutive Aspects of Concrete Failure", *Spec. Publ. Finite Element Analysis of Concrete Structures*, ASCE Spec. Publ., NY., pp. 226–254.

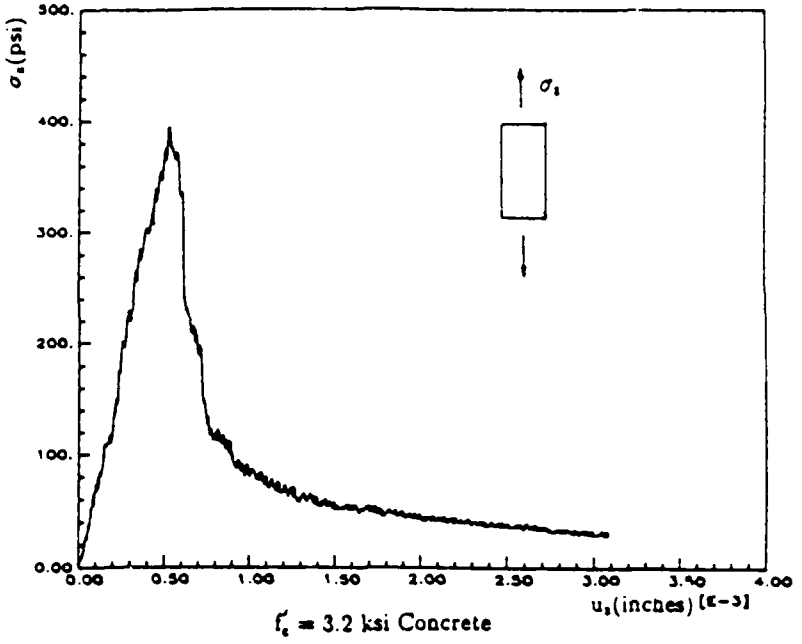

f'_c = 3.2 ksi Concrete

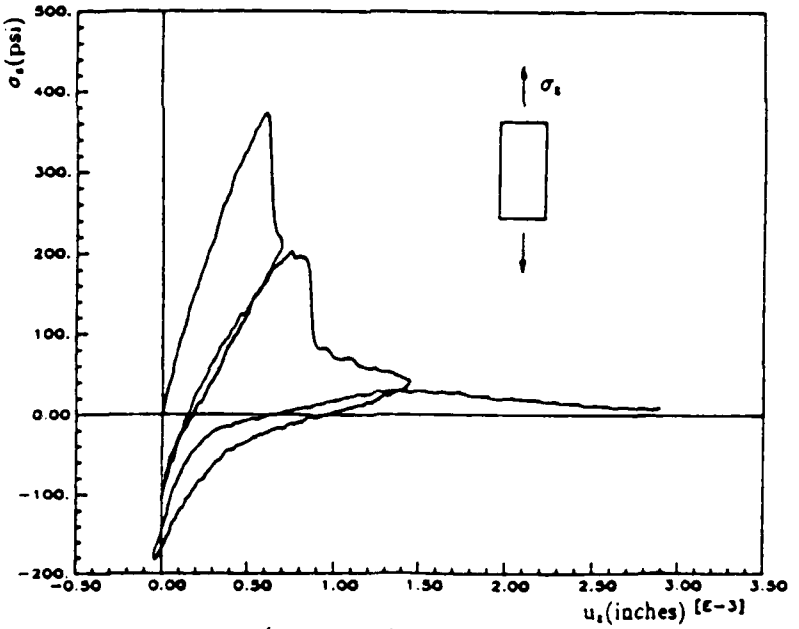

f'_c = 3.2 ksi Concrete

Fig. 1 Direct Tension Experiments by B. Hurlbut[6]

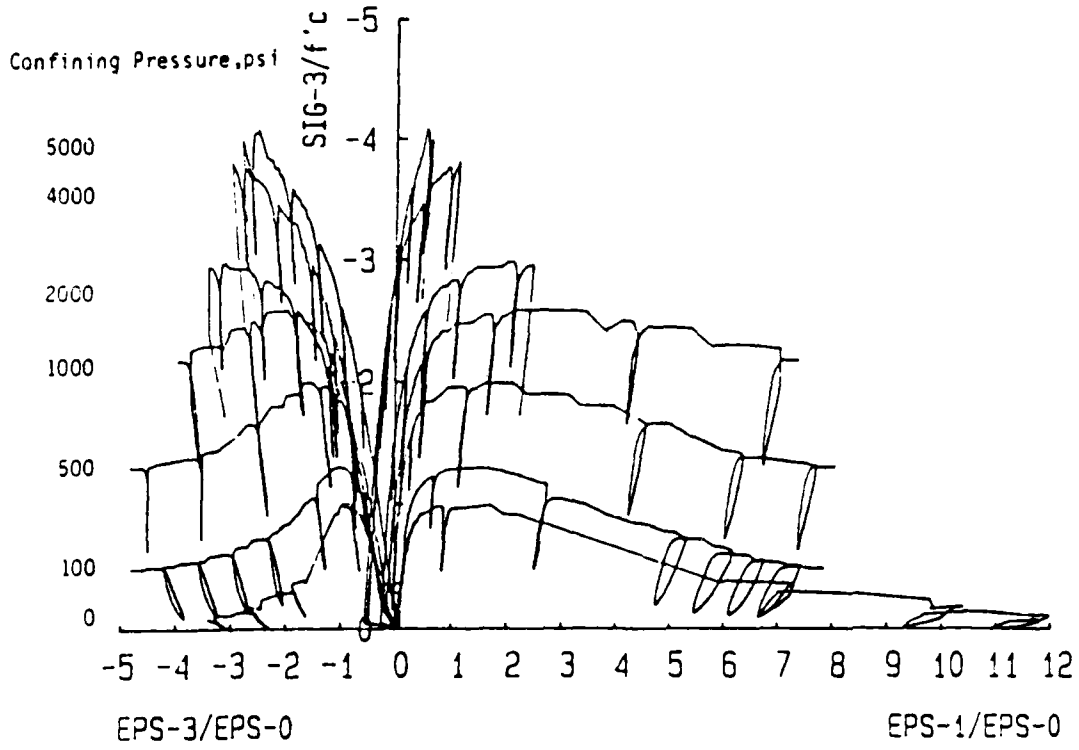

Fig. 2 Triaxial Compression Experiments by S. Smith[8]

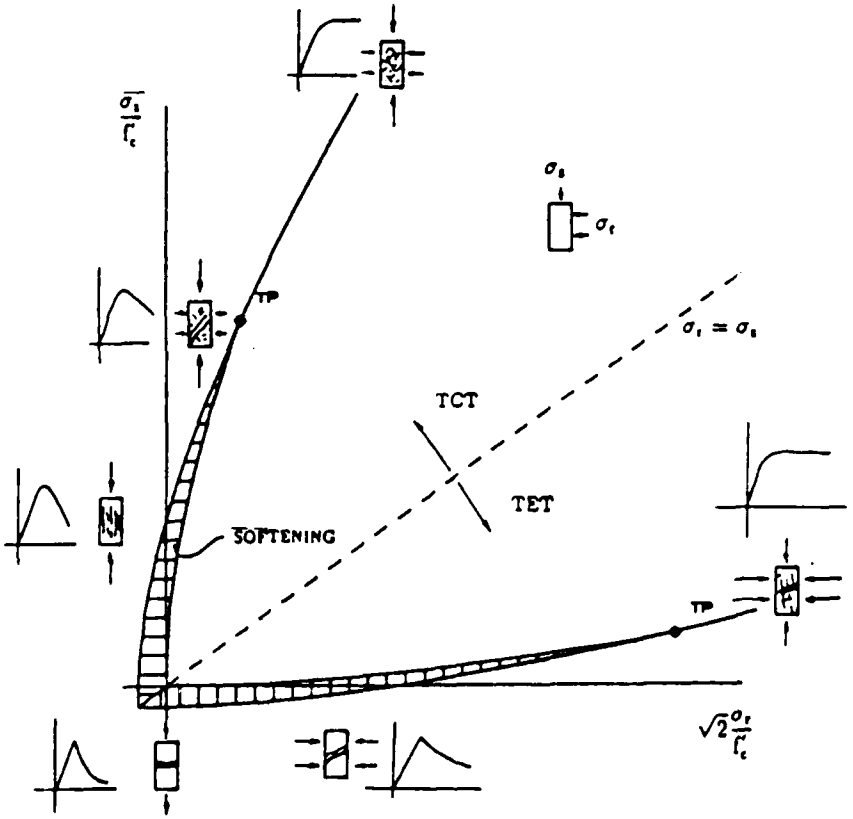

Fig. 3 Failure Modes in Triaxial Compression and Extension

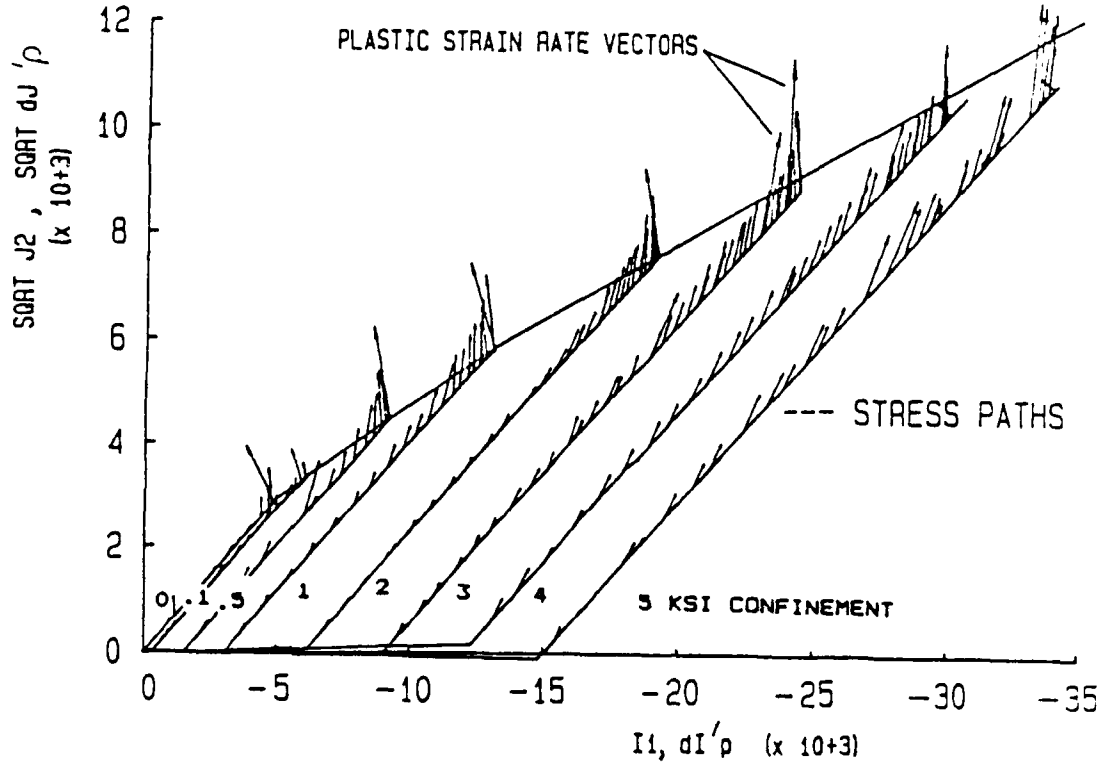

Fig. 4 Incremental Plastic Strains Superposed on Triaxial Stress Path

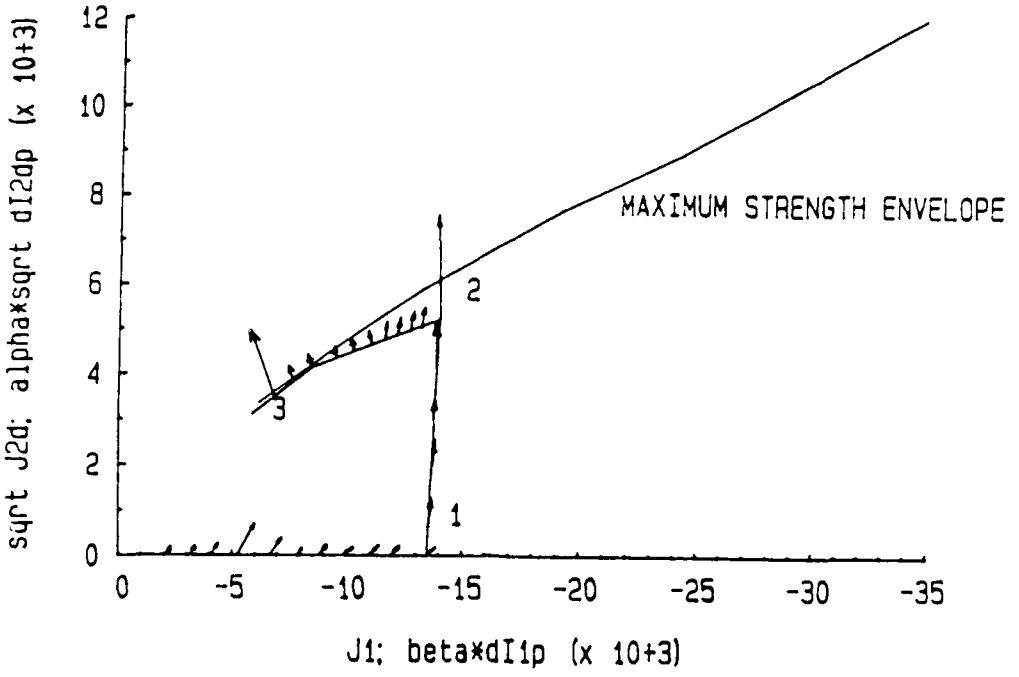

Fig. 5 Wedge Experiment: Stress Path and Incremental Plastic Strain Vectors

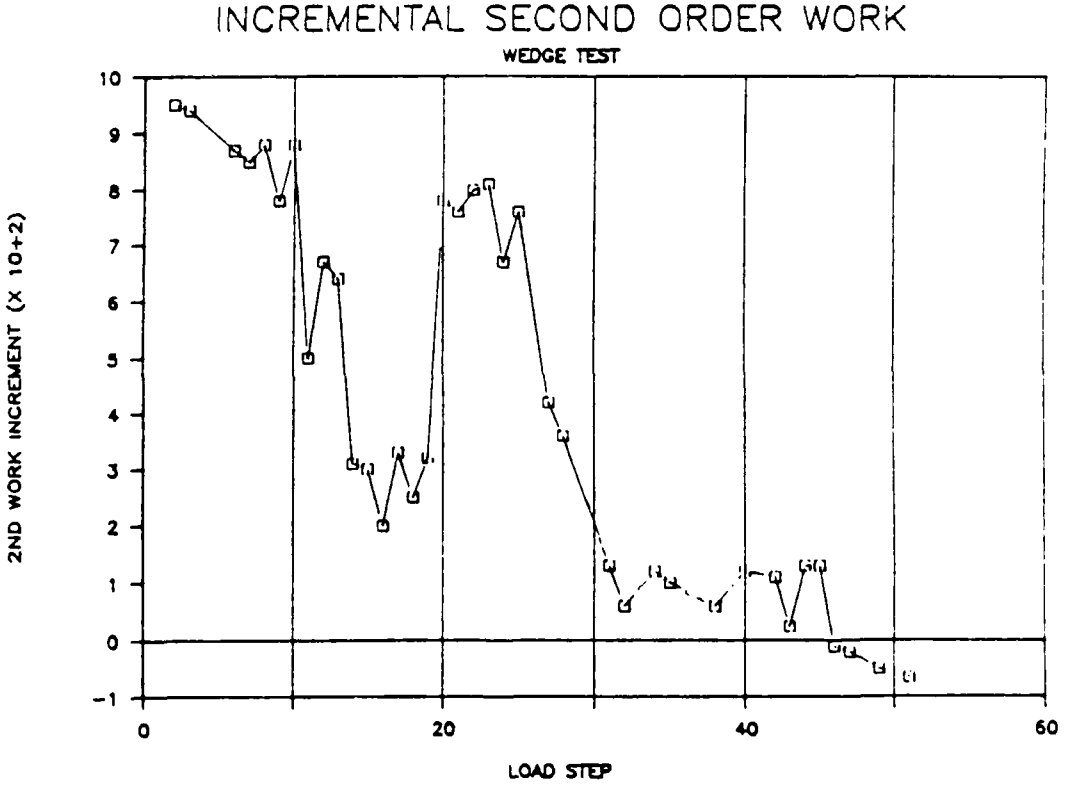

Fig. 6 Incremental Plastic Work at Different Stages of Wedge Experiment

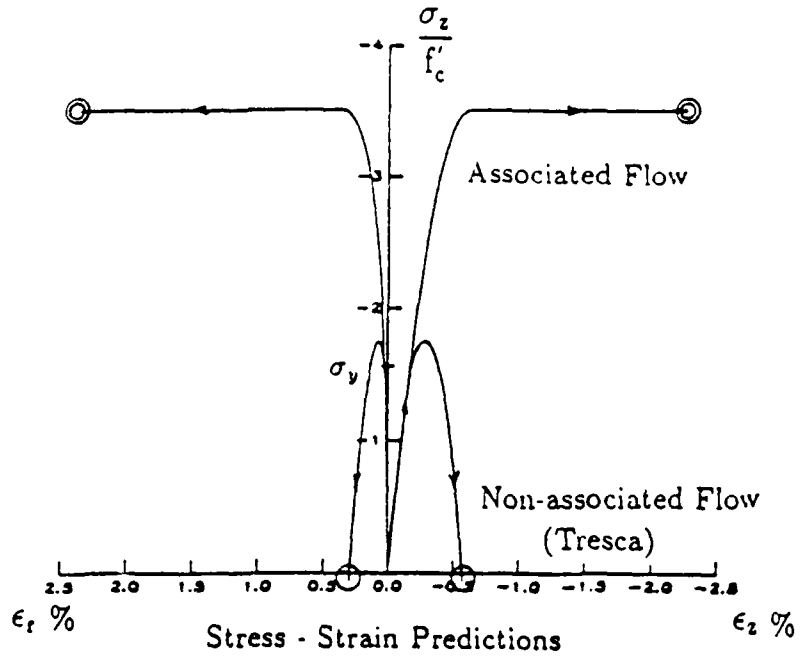

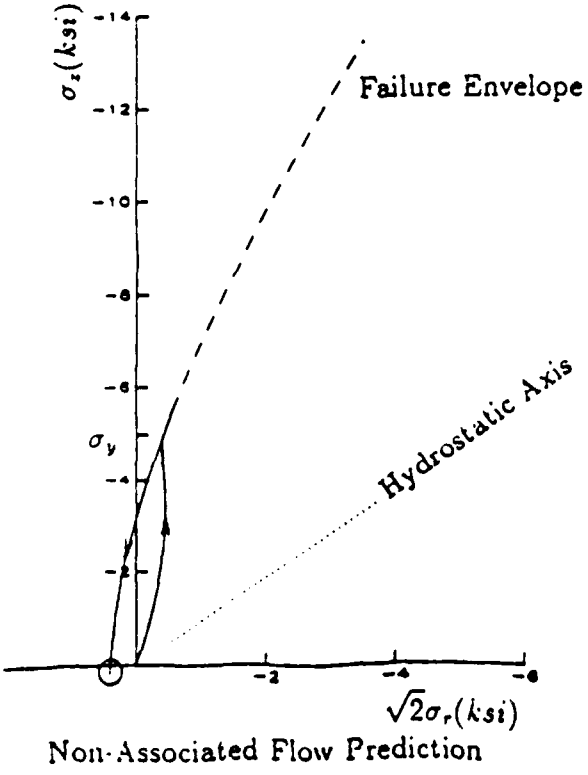

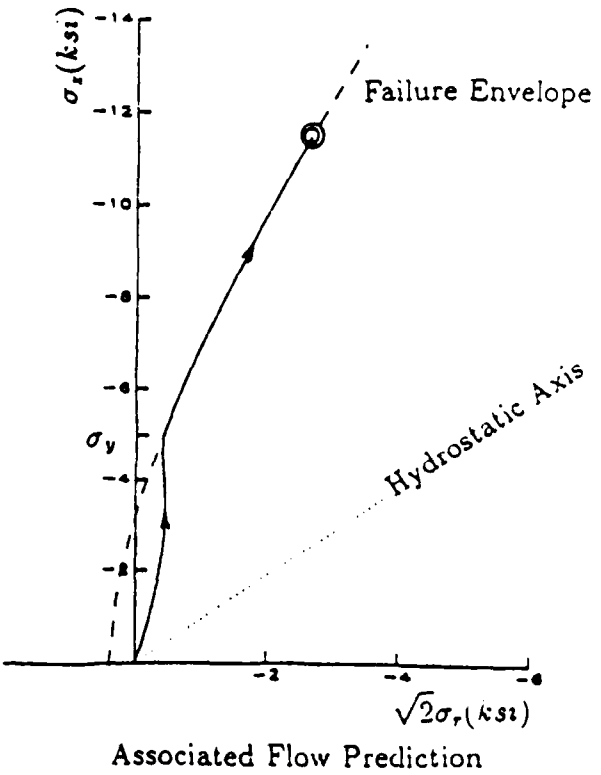

Fig. 7 Difference of Associated and Non-Associated Flow Predictions

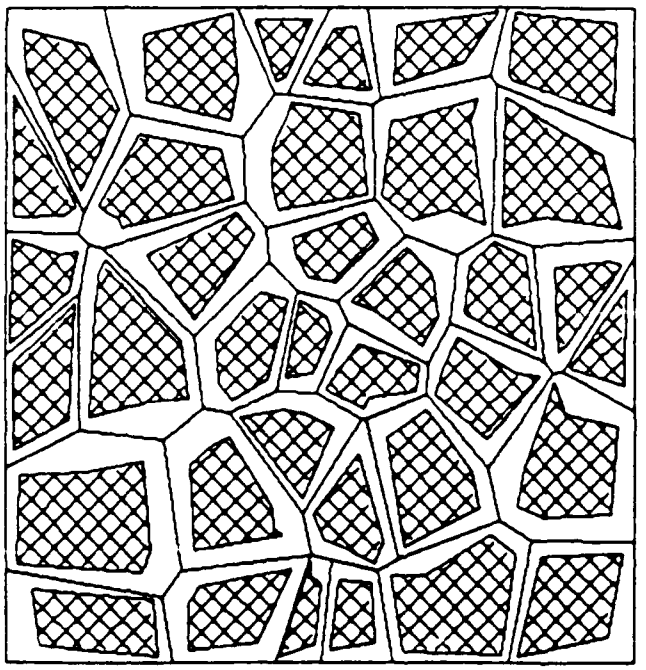

Fig. 8 Non-Contiguous Polygonal Structure of Concrete Composite

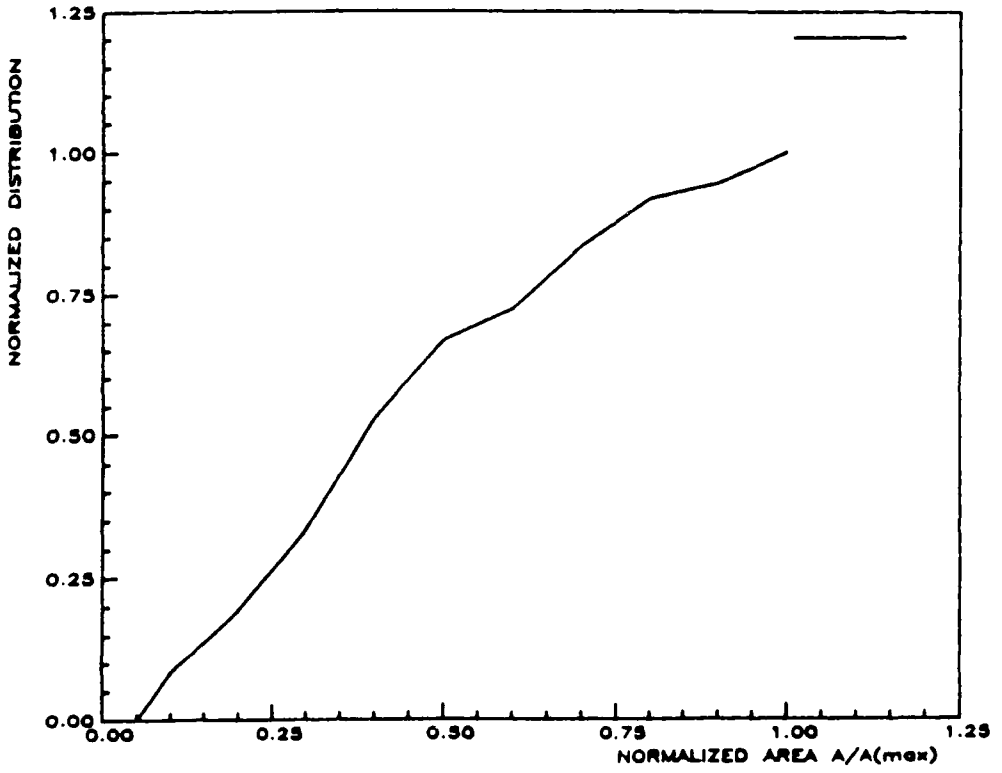

Fig. 9 Cumulative Size Distribution of Aggregate Phase

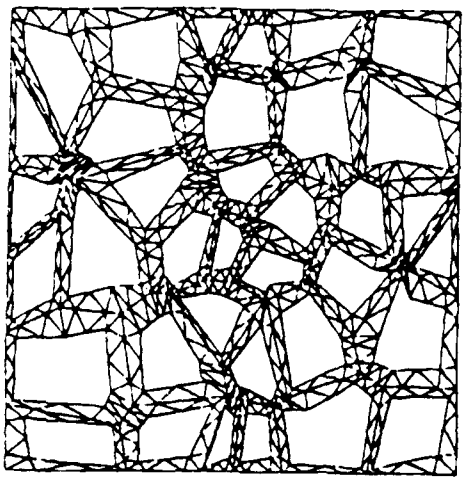

Triangulation of Mortar Phase

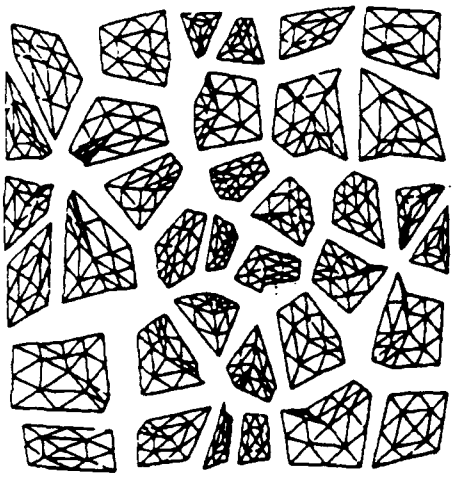

Triangulation of Aggregate Phase

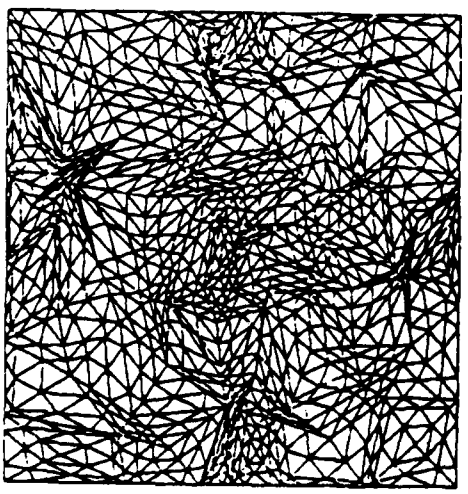

Fig. 10 Triangulation of Mortar-Aggregate Composite

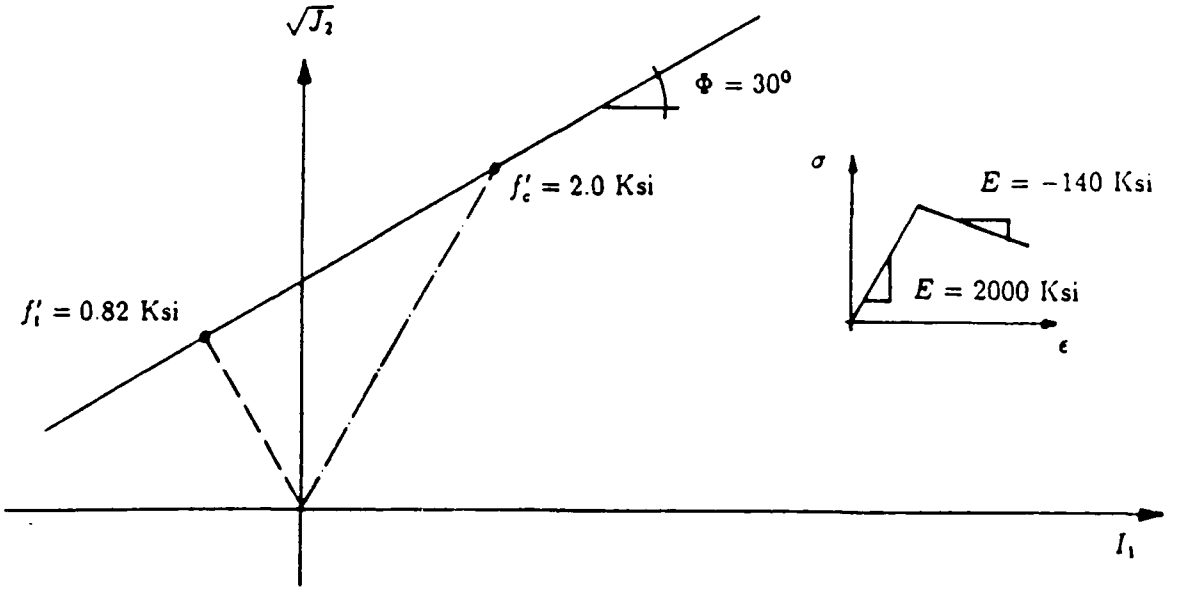

Fig. 11 Decohesive Drucker-Prager Description of Mortar Phase

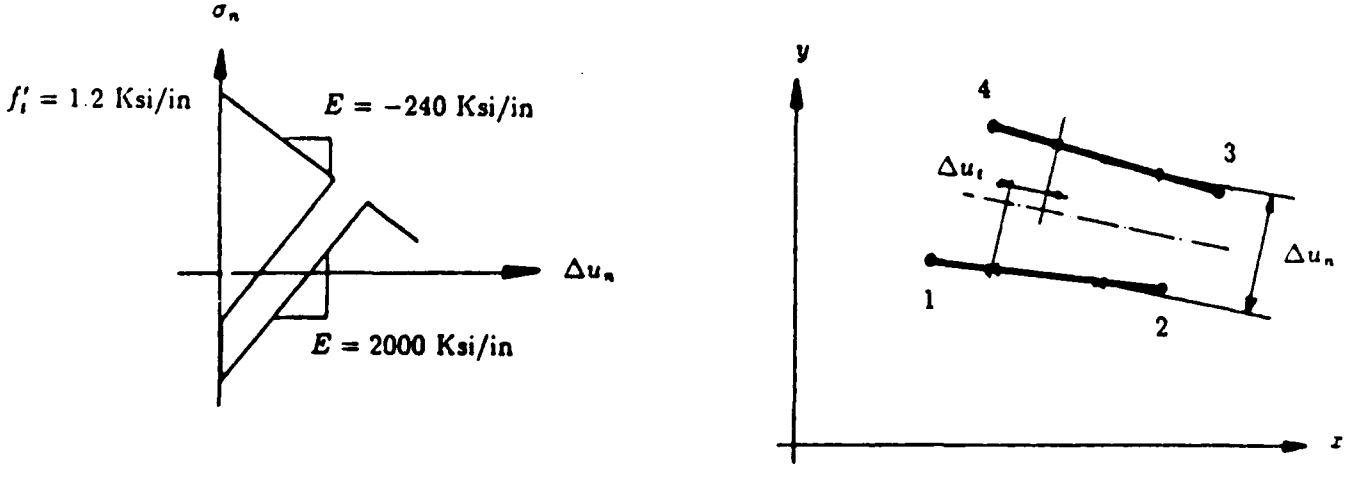

Fig. 12 Interface Element for Tensile Debonding of Mortar-Aggregate Contact

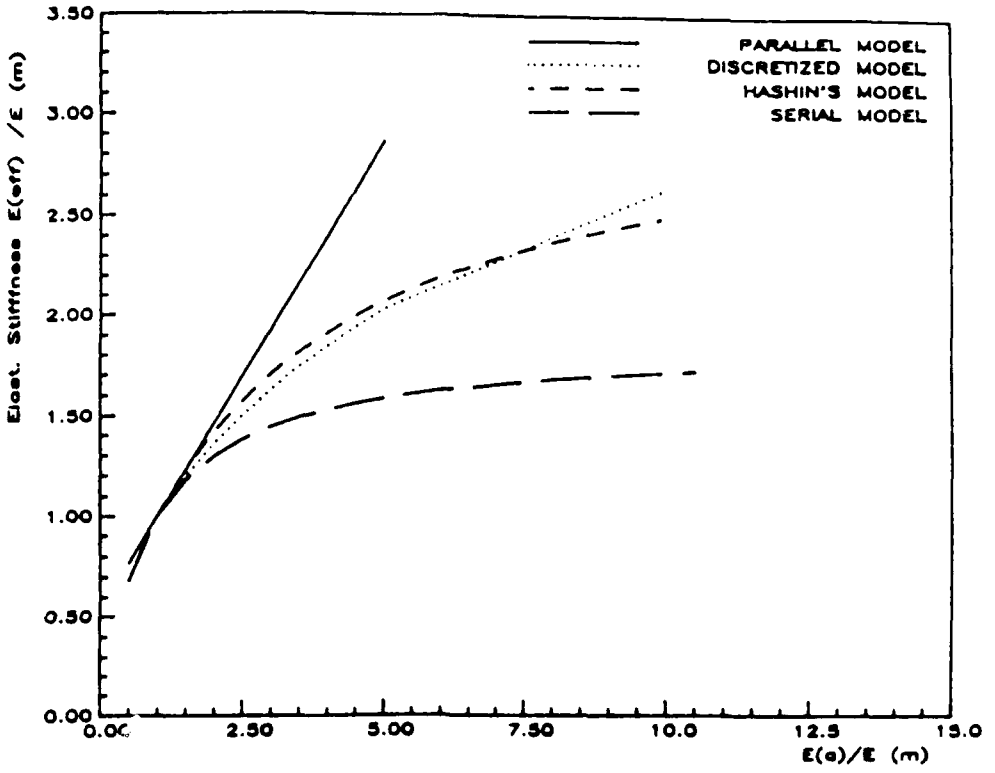

Fig. 13 Effective Elastic Properties of Particulate Composite

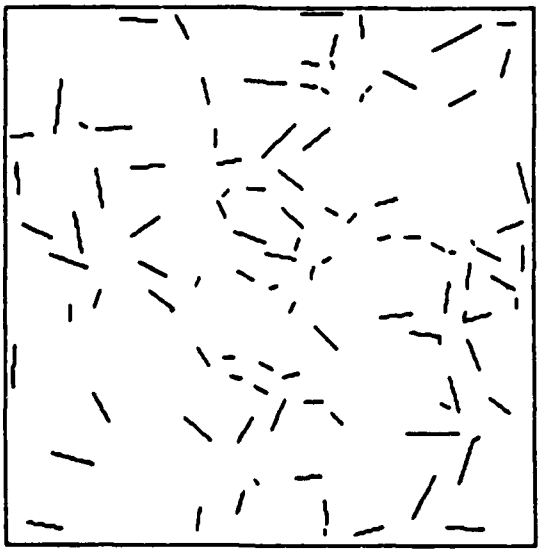

Fig. 18 Tensile Failure Pattern of Interface Debonding at 75% Peak Strength

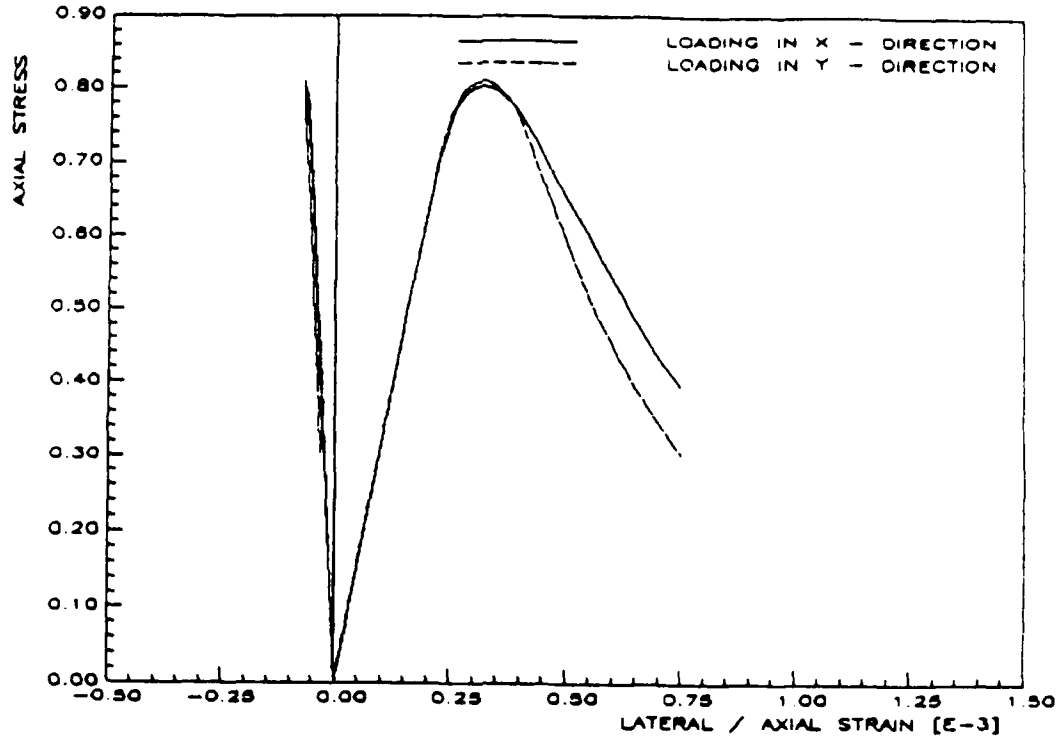

Fig. 14 Isotropy of Stiffness and Strength in Uniaxial Tension

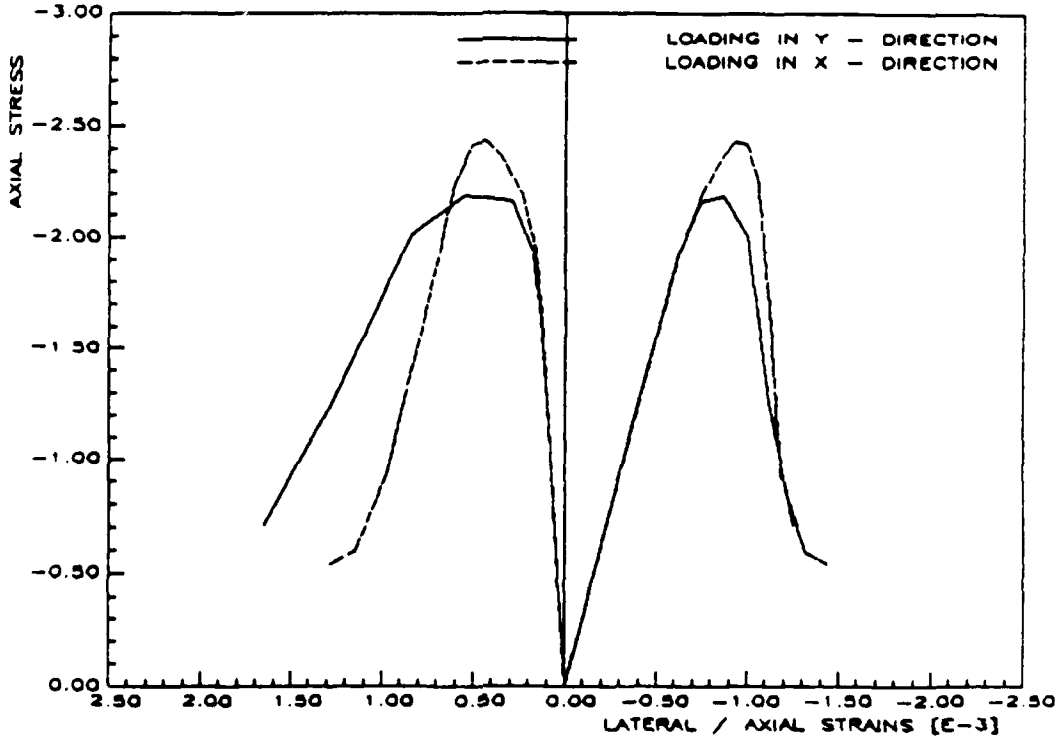

Fig. 15 Isotropy of Stiffness and Strength in Uniaxial Compression

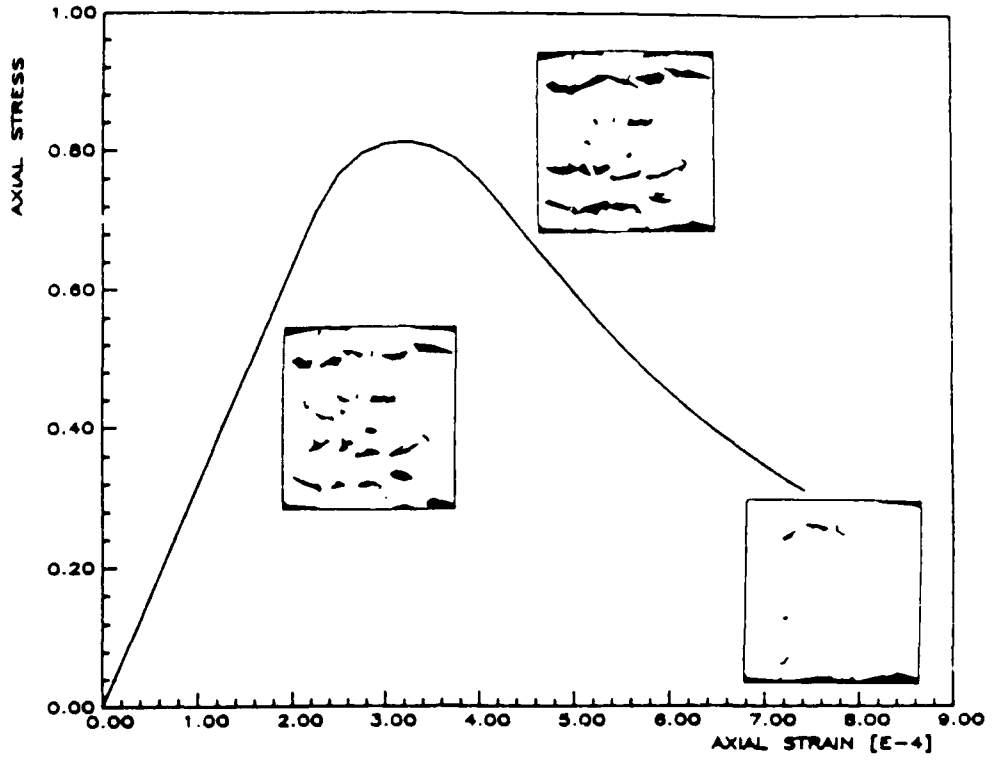

Fig. 16. Progressive Failure Behavior in Direct Tension Experiment

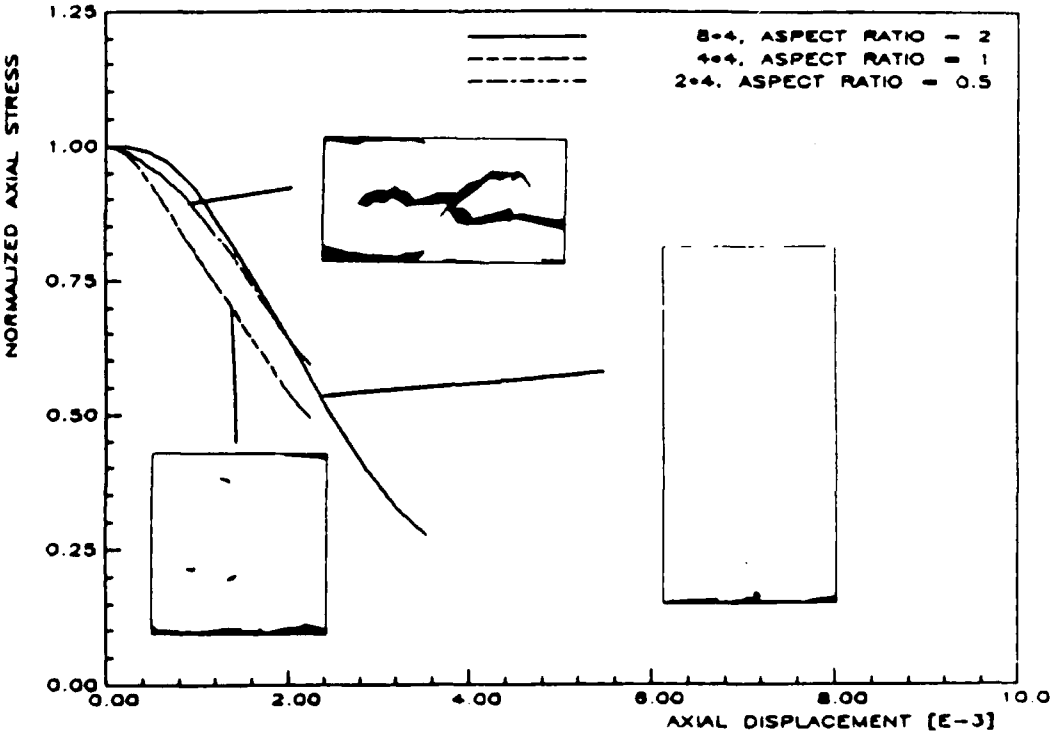

Fig. 17 Post-Peak Behavior of Different Height Tension Specimens

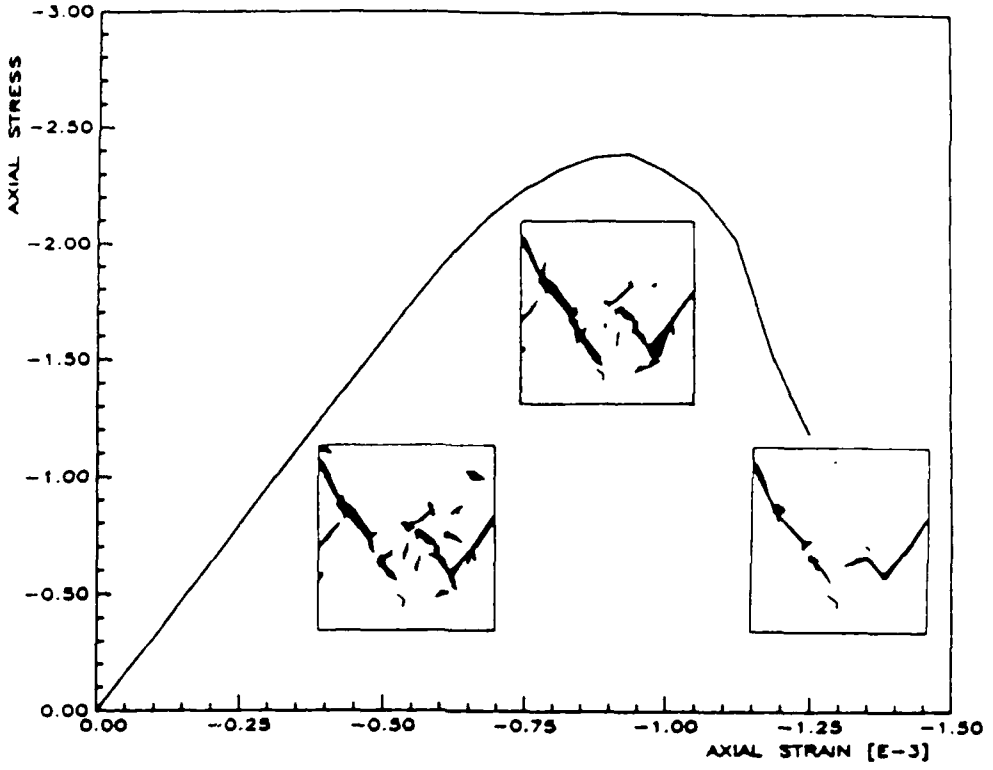

Fig. 19 Progressive Failure Behavior in Uniaxial Compression

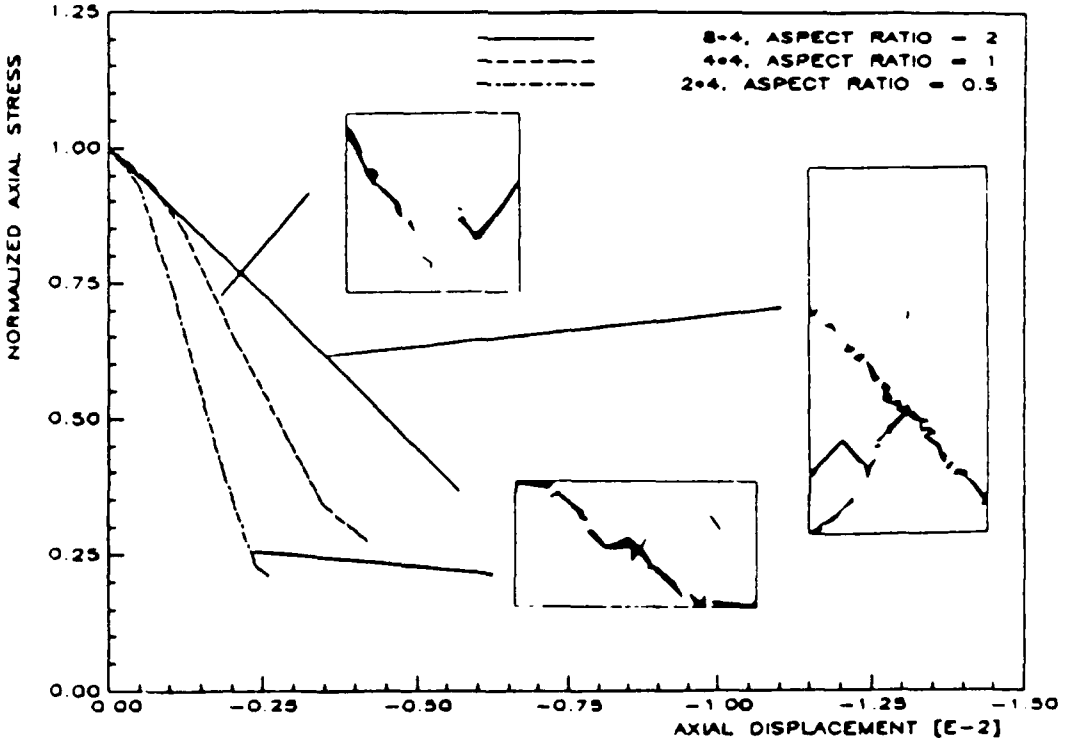

Fig. 20 Post-Peak Behavior of Different Height Compression Specimens

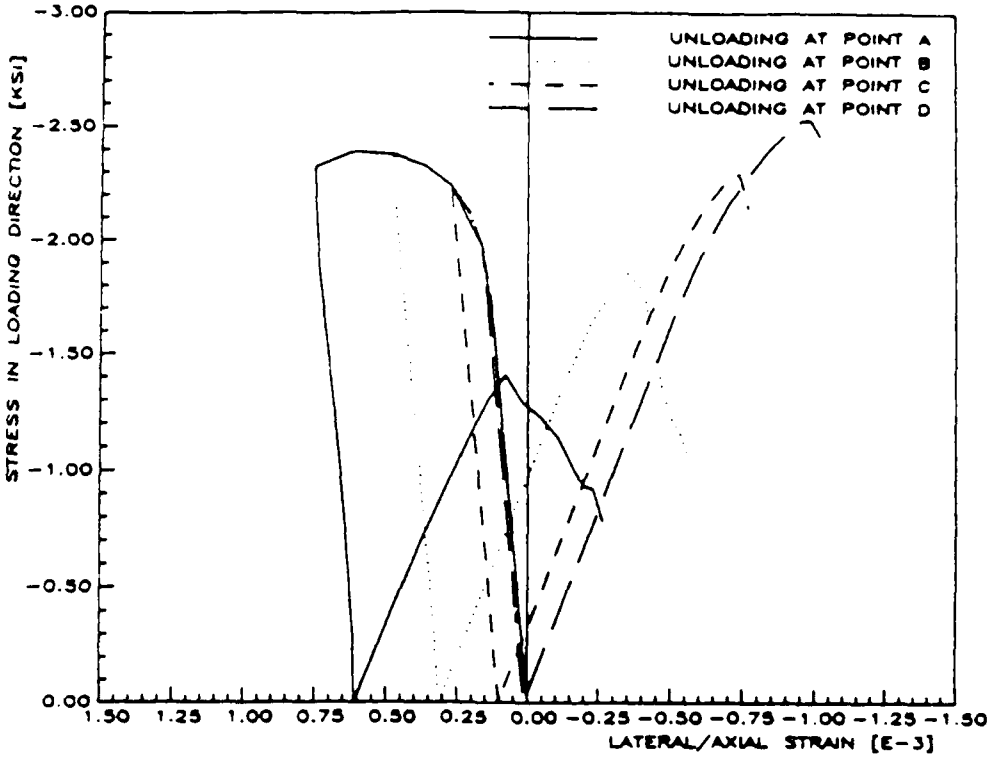

Fig. 21 Compressive Strength Degradation due to 90^0 Preloading in Compression

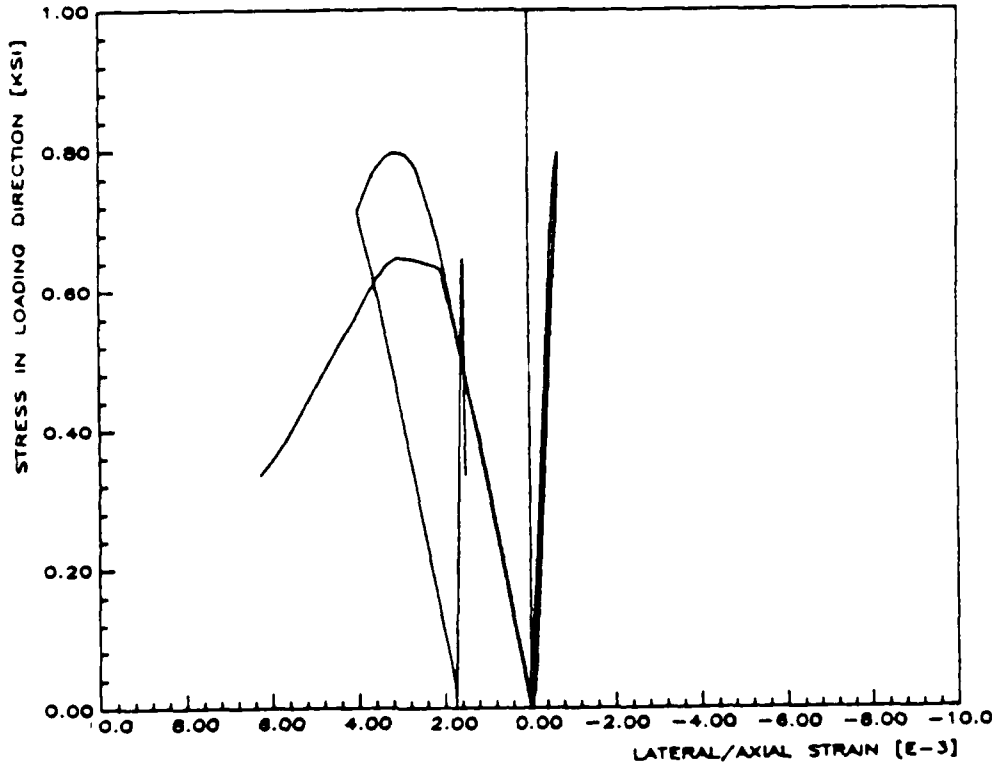

Fig. 22 Tensile Strength Degradation due to 90^0 Preloading in Tension

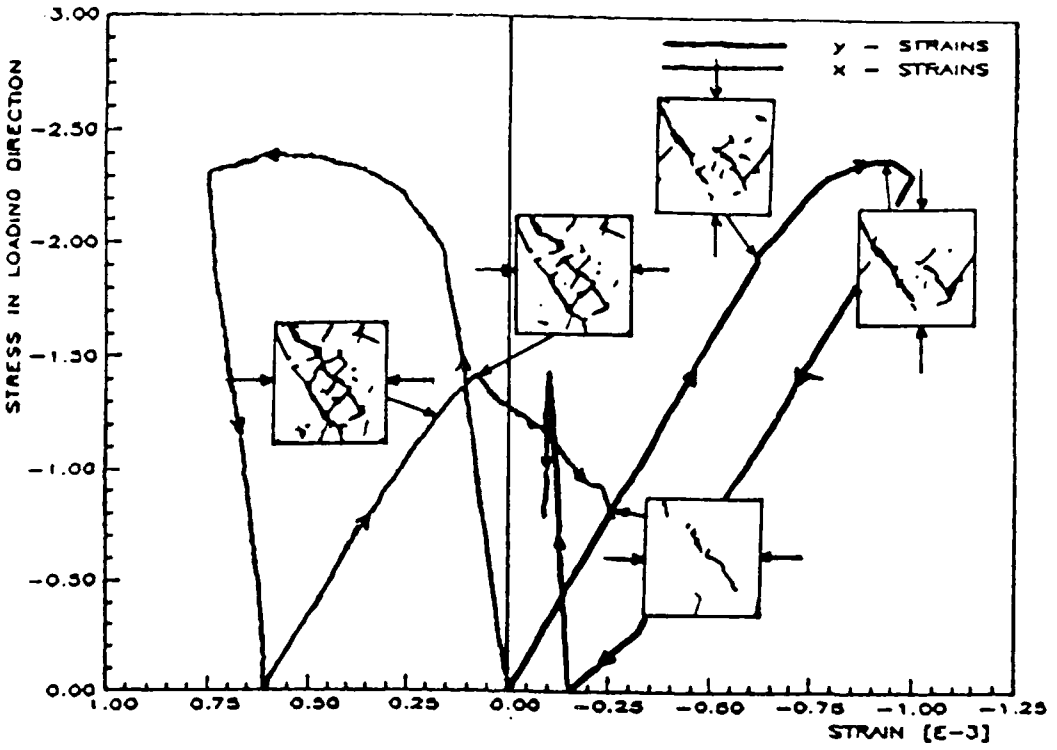

Fig. 23 Summary of Load History Experiments in Compression

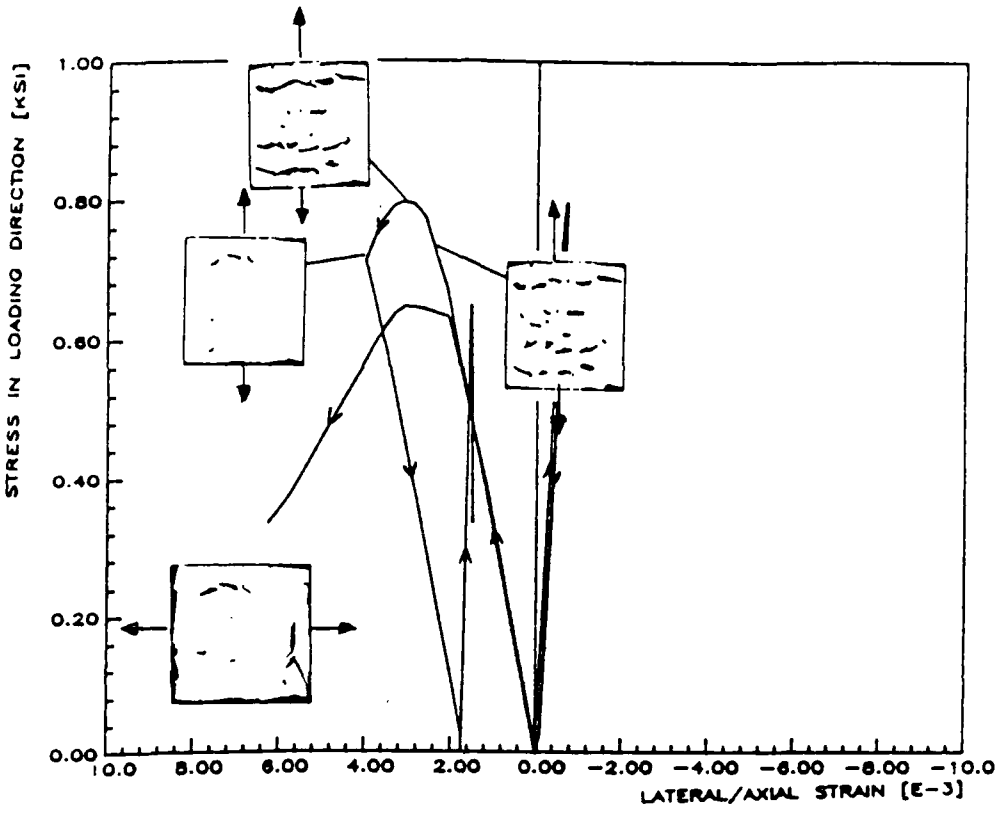

Fig. 24 Summary of Load History Experiments in Tension